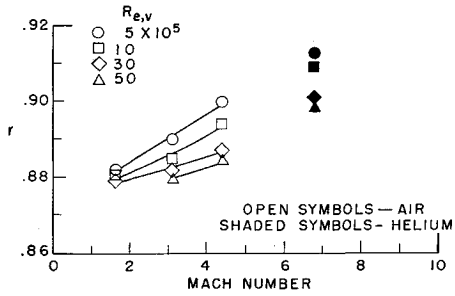

Fig. 4 Effect of Mach number on turbulent recovery factor.

test the ratio of the measured surface temperature to the total temperature changed less than 0.35% for each wire. Recovery factors were then calculated using the equilibrium surface temperature as adiabatic-wall temperature in the defining equation for recovery factor.

The results of the test are shown in Fig. 2. No data were obtained in the laminar region; however, the theoretical values for the helium recovery factor predicted by laminar similar solutions[14] at Mach 6.8 is indicated. The approximate beginning of the transition region determined from heat-transfer tests with unheated flow[15] using a thin metal plate mounted on the same wedge model at similar test conditions is also shown. In Ref. 15 the end of the transition region was found to be located at a distance approximately twice as far from the leading-edge as the beginning. Based on these Ref. 15 results, the first data point is believed to be in the transition region near the location of the peak in recovery factor. This trend is consistent with previous air measurements such as the data of Mack[9] shown in Fig. 2 for comparison. Based on the fairing through the data, the turbulent helium recovery factor at high Reynolds numbers and Mach 6.8 is approximately 0.899 ± 0.002. This is significantly higher than the generally used value of 0.883 (cube root of the molecular Prandtl number).

To investigate the effect of Reynolds number and Mach number on the turbulent recovery factor previous air measurements were examined. Fig. 3 shows, for several Mach numbers, the measured recovery factor as a function of Reynolds number based on distance from the location of the peak values in the transition region. As shown in Fig. 3, all the data for each Mach number follow the same trend, with the recovery factor dropping rapidly from a peak value to a slightly decreasing value at higher Reynolds numbers.

The data at several Reynolds numbers are cross plotted in Fig. 4 as a function of Mach number. In contrast to the theory of Tucker and Maslin,[16] the data indicate that the turbulent recovery factor increases with increasing Mach number.

References

[1] Brinich, P. F., "Recovery Temperature, Transition, and Heat Transfer Measurements at Mach 5," TN D-1047, Aug. 1961, NASA.

[2] Dmohoski, S. M., "Temperature Recovery Factors on a 40-Degree Cone Cylinder with Turbulent Boundary Layer at Mach Numbers 4.1 and 4.8," NAVORD Rept. 5763, Aug. 1957, U.S. Naval Ordnance Lab., White Oak, Md.

[3] Jack, J. R., and Moskowitz, B., "Experimental Investigation of Temperature Recovery Factors on a 10° Cone at Angle of Attack at a Mach Number of 3.12," TN 3256, July 1954, NACA.

[4] Shoulberg, R. H., Hill, J. A. F., and Rivas, J. M. A., Jr., "An Experimental Determination of Flat Plate Recovery Factors for Mach Numbers Between 1.90 and 3.14," M.I.T. Wind Tunnel Rept. 36, May 1952, M.I.T., Cambridge, Mass.

[5] Stine, H. A., and Scherrer, R., "Experimental Investigation of the Turbulent Boundary Layer Temperature-Recovery Factor on Bodies of Revolution at Mach Numbers from 2.0 to 3.8," TN-2664, March 1952, NACA.

[6] Stalder, J. R., Rubesin, M. W., and Tendeland, T., "A Determination of the Laminar-, Transitional-, and Turbulent-Boundary Layer Temperature Recovery Factors on a Flat Plate in Supersonic Flow," TN-2077, June 1950, NACA.

[7] Brinich, P. F., "Boundary Layer Transition at Mach 3.12 With and Without Single Roughness Elements," TN 3267, 1954, NACA.

[8] Evvard, J. C., Tucker, M., and Burgess, W. C., Jr., "Statistical Study of Transition-Point Fluctuations in Supersonic Flow," TN 3100 1954, NACA.

[9] Mack, L. M., "An Experimental Investigation of the Temperature Recovery Factor," Rept. 20-80, Aug. 1954, Jet Propulsion Lab., Pasadena, Calif.

[10] Tendeland, T., "Effects of Mach Number and Wall-Temperature Ratio on Turbulent Heat Transfer at Mach Numbers from 3 to 5," TR R-16, 1959, NASA.

[11] DeLauer, R. D. and Nagamatsu, H. T., "Experimental Heat Transfer at Hypersonic Mach Numbers," Memo 14, April 1953, California Institute of Technology, Guggenheim Aeronautical Lab., Pasadena, Calif.

[12] Reller, J. O., Jr. and Hamaker, Frank M., "Temperature Recovery Factors on a Slender 12° Cone Cylinder at Mach Numbers from 3.0 to 6.3 and Angles of Attack up to 45°," R&M A55G20, Oct. 1955, NACA.

[13] Nicoll, K. M., "An Experimental Investigation of Laminar Hypersonic Cavity Flows," Part II: "Heat Transfer and Recovery Factor Measurements," ARL Rept. 63-73, Jan. 1964, Wright-Patterson Air Force Base, Ohio.

[14] Nicoll, K. M., "Investigation of the Laminar Boundary-Layer on a Flat Plate in Helium Using the Crocco Method," ARL Rept. 62-345, May 1962, Wright-Patterson Air Force Base, Ohio.

[15] Wagner, R. D., Jr., et al., "Influence of Measured Free-Stream Disturbances on Hypersonic Boundary Layer Transition," AIAA Paper 69-704, San Francisco, Calif., 1969.

[16] Tucker, M. and Maslen, S. H., "Turbulent Boundary-Layer Temperature Recovery Factors in Two-Dimensional Supersonic Flow," TN 2296, 1951, NACA.

Nonlinear Elastic Response of an Incased Tubular Grain

ROGER J. EVANS*

AND

MICHAEL S. HAYCOCK†

University of Washington, Seattle, Wash.

Introduction

THE mechanical response of highly loaded solid propellants is significantly nonlinear at strain levels of 5 or 10% in uniaxial stress states. A previous paper in this Journal[1] has shown that useful results may be obtained from the stress analysis of elastic solids that are physically nonlinear conditions of geometric linearity. Solutions were presented for the internal pressurization of a rigidly incased tubular grain and for thermal stresses in an incased grain.

Baltrukonis and Vaishnev[2] considered finite axisymmetric deformations with regard to the analysis of solid propellant grains. Their work, however, was restricted to a particular class of incompressible elastic solids.

The purpose of this Note is to extend the analysis of Pister and Evans[1] to the more realistic case: where the problem formulation takes into account both physical and geometric nonlinearity. Such an extension is of importance with regard both to extending the range of useful solutions and to justifying the simultaneous consideration of geometric linearity and physical nonlinearity. Solutions for geometric

Received June 24, 1970; revision received September 8, 1970.

* Assistant Professor, Department of Civil Engineering.

† Graduate Student, Department of Civil Engineering.

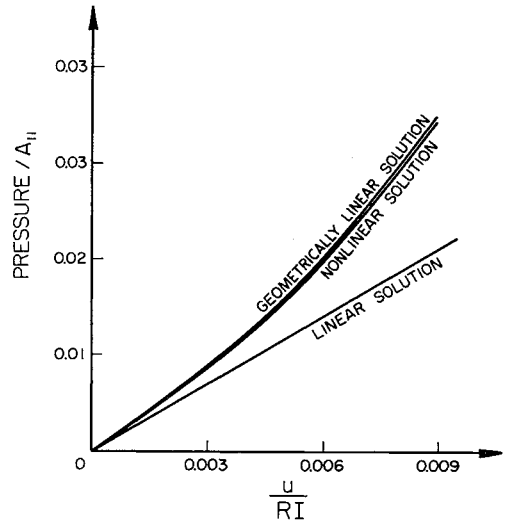

Fig. 1 Pressure-bore displacement relation: $A_{22}/A_{11} = -30$.

linearity and physical nonlinearity are obtained by solving the completely nonlinear problem and subsequently considering the special case where displacement gradients are small compared with unity.

The displacement equation of equilibrium for nonlinear axisymmetric plane strain is derived and is then used to find the state of stress and displacement for an internally pressurized tubular grain. Effects of physical and geometric nonlinearity are isolated separately, and the results are compared with those of Pister and Evans[1] in which geometric nonlinearity was omitted.

Governing Equation for Axisymmetric Plane Strain

Several alternative definitions for stress and strain are available for the nonlinear problem. The Lagrangian formulation together with Kirchoff stress[3] is used here. An advantage of this is that the hyperelastic constitutive law has the simple form

$$S_{ij} = \partial U/\partial L_{ij} \tag{1}$$

where S_{ij} is the Kirchoff stress, U the internal energy density per unit mass, and L_{ij} is the Lagrange or material strain tensor. L_{ij} is defined by

$$L_{ij} = \tfrac{1}{2}(u_{i|j} + u_{j|i} + \delta u^k{}_{|i} u_{k|j}) \tag{2}$$

where u_i is the displacement, and the vertical line means covariant differentiation with respect to the material coordinate a^i. δ is a tracer to identify terms due to geometrical nonlinearity: δ is $+1$ in general but is set equal to zero when geometry nonlinearity is omitted. In the absence of body forces, the equations of equilibrium in terms of S_{ij} are

$$[(\partial x^k/\partial a^m)S^{mn}]_n = 0 \tag{3}$$

where x^i is the spatial coordinate.

For boundary conditions where traction is specified as well as for physical interpretation, physical components of stress, $\sigma_{\langle ij\rangle}$ are required. These are related to the Kirchoff stress by

$$\sigma_{\langle ij\rangle} = \left(\frac{\rho}{\rho_0}\right)(g_{ii})^{1/2}(g_{jj})^{1/2}\frac{\partial x^i}{\partial a^p}\frac{\partial x^j}{\partial a^q}S^{pq} \qquad \text{(no sum on } i,j\text{)}$$

where g_{ij} is the covariant metric, ρ is the spatial density, and ρ_0 is the material density.

The displacement equations of equilibrium are obtained by substituting Eqs. (1) and (2) into Eq. (3). The particular form of constitutive law used here is

$$S_{ij} = A_{11}L_k{}^k g_{ij} + A_{12}L_{ij} + A_{22}L_m{}^k L_k{}^m g_{ij} + 2A_{22}L_k{}^k L_{ij} \tag{4}$$

this being consistent with that of Pister and Evans. The resulting displacement equation of equilibrium for axisym-

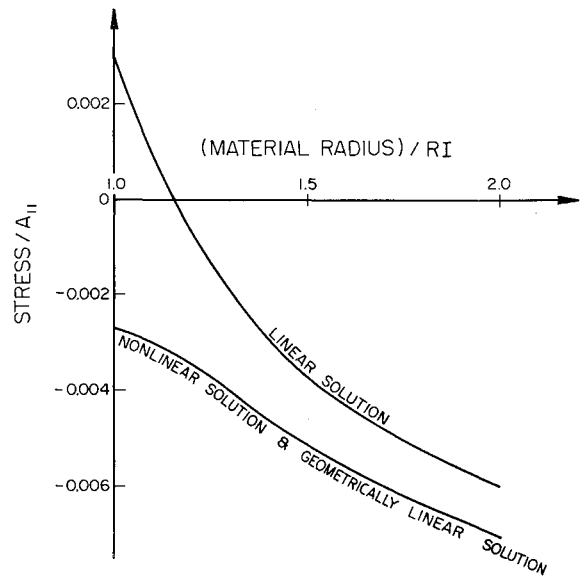

Fig. 3 Circumferential stress distribution: $A_{22}/A_{11} = -30$.

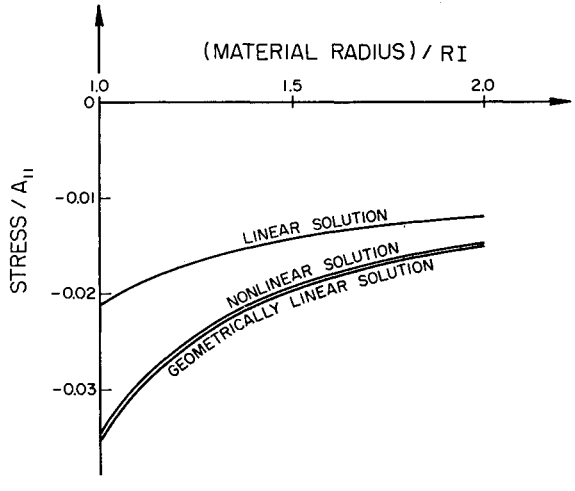

Fig. 2 Radial stress distribution: $A_{22}/A_{11} = -30$.

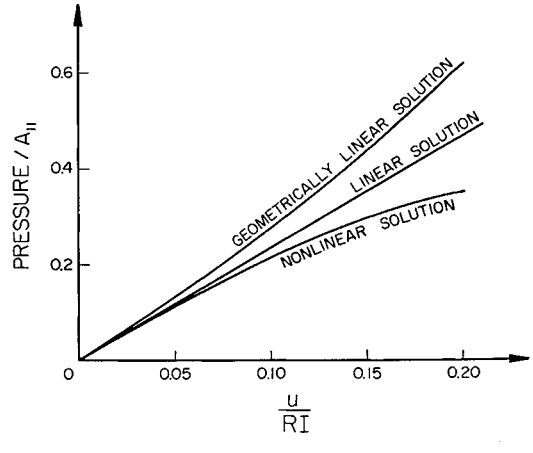

Fig. 4 Pressure-bore displacement relations: $A_{22}/A_{11} = -\frac{2}{3}$.

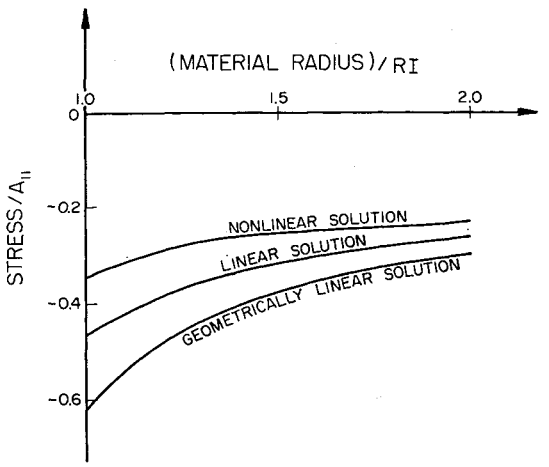

Fig. 5 Radial stress distribution: $A_{22}/A_{11} = -\frac{2}{3}$.

metric plane strain is then

$$[(A_{11} + A_{12})\alpha' + A_{11}\beta' + (A_{12}/r)\ (\alpha - \beta)] + (\delta u''/\delta u' + 1)\ [(A_{11} + A_{12})\alpha + A_{11}\beta + 3A_{22}\alpha^2 + A_{22}(2\alpha\beta + \beta^2)] + [6A_{22}\alpha\alpha' + 2A_{22}(\alpha\beta' + \beta\alpha' + \beta\beta')\ 2\ (A_{22}/r)\ (\alpha^2 - \beta^2)] = 0 \quad (5)$$

where

$$\alpha = u' + \frac{\delta}{2}(u')^2,\ \beta = \frac{u}{r} + \frac{\delta}{2}\left(\frac{u}{r}\right)^2,\ (\ )' = \frac{d(\ )}{dr}$$

In the preceding, u is the radial displacement and r is the material radius.

Some quantitative measure of nonlinearity is required. While this is somewhat arbitrary, the definition of Pister and Evans for physical nonlinearity is used, i.e.,

$$k_p = 3A_{22}u/r(A_{11} + A_{12})$$

while, for geometric nonlinearity the measure used is

$$k_g = u/r$$

Ignoring geometric nonlinearity is equivalent to setting

$$\delta = 0,\ \partial x^i/\partial a^i = \delta_j{}^i$$

in Eq. (5).

Internal Pressurization of an Incased Tubular Grain

Pressurization of a rigidly incased grain of initial inner radius RI and outer radius RO is considered.

The boundary conditions are

$$u(r = RO) = 0,\ \sigma_{(rr)}(r = RI) = -P$$

where P is the applied pressure.

For computation purposes and for comparison with the results of Pister and Evans, the following data has been used: $RI = 1.0$, $RO = 2.0$, $A_{11} = A_{12}$.

The computational procedure used Newton's method with finite differences as described by Pister and Evans, and this will not be discussed further here.

In Figs. 1–3, results are shown for $A_{22}/A_{11} = -30.0$; this corresponding to a material which hardens in compression. Figure 1 shows the relation of pressure to bore displacement up to $u(RI) = 0.009$, while in Figs. 2 and 3 distributions of radial and circumferential stress are shown for $u(RI) = 0.009$. Solutions corresponding to geometric linearity as well as those for both geometric and physical linearity are also shown on these figures. For the particular data given, the geometrically linear case corresponds to that of Pister and Evans, and it may be seen that the error due to omitting geometrically nonlinear terms is slight. This is, in fact, to be expected since for

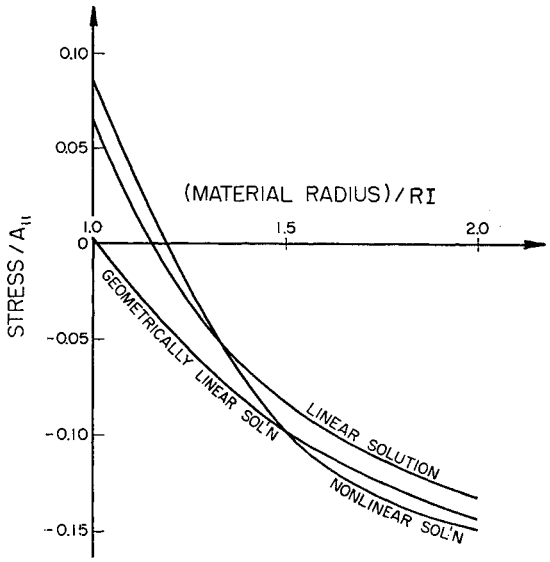

Fig. 6 Circumferential stress distribution: $A_{22}/A_{11} = -\frac{2}{3}$.

$$A_{22}/A_{11} = -30.0 \text{ and } u(RI) = 0.009, \text{ at } r = RI$$

$$k_p = -0.40,\ k_g = 0.009$$

Results for another case are shown in Figs. 4–6: here $A_{22}/A_{11} = -\frac{2}{3}$.

In Fig. 4, pressure is plotted against bore displacement for $u(RI)$ from 0 to 0.20. Within this range, Newton's method was found to give accurate solutions to Eq. (5). Figures 5 and 6 show the distribution of radial and circumferential stress at $u(RI) = 0.20$. For this bore displacement at $r = RI$

$$-k_p = k_g = 0.20$$

The effect of including geometric nonlinearity is, in this case, seen to be significant and, in fact, to change the nonlinear nature of the pressure/bore displacement relation from hardening with increased displacement to softening.

Conclusions

A particular elastic problem has been solved taking into account both physical and geometric nonlinearity. It has been demonstrated that each nonlinearity may have a significant effect on the state of stress and on the load deformation characteristics. In addition, the procedure of considering physical nonlinearity together with geometric linearity has been shown to be valid when the displacement gradients are small compared with unity.

References

[1] Pister, K. S. and Evans, R. J., "Stress Analysis for Elastic Response of Physically Nonlinear Solid Propellants," *AIAA Journal*, Vol. 4, No. 11, Nov. 1966, pp. 1914–1919.

[2] Baltrukonis, J. H. and Vaishnav, R. N., "Finite Deformations Under Pressurization in an Infinitely Long, Thick Walled, Elastic Cylinder Ideally Bonded to a Thin Elastic Case," *Transactions of the Society of Rheology*, Vol. 9, No. 1, 1965, pp. 273–291.

[3] Noll, W. and Truesdell, C. A., "The Non-linear Field Theories of Mechanics," *Handbuch der Physik*, Vol. 3, Pt. 3 Springer, Berlin.